Applied Surface Science 347 (2015) 23–34

Contents lists available at ScienceDirect

Applied Surface Science

journal homepage: www.elsevier.com/locate/apsusc

CoCrMo alloy for orthopedic implant application enhanced corrosion and tribocorrosion properties by nitrogen ion implantation

Zijian Guo [a], Xiaolu Pang [a,b,*], Yu Yan [c], Kewei Gao [a], Alex A. Volinsky [d], Tong-Yi Zhang [b]

[a] Materials Science and Engineering, University of Science and Technology Beijing, Beijing, 100083, People's Republic of China
[b] Department of Mechanical Engineering, The Hong Kong University of Science and Technology, Clear Water Bay, Kowloon, Hong Kong, China
[c] Corrosion and Protection Center, Key Laboratory for Environmental Fracture (MOE), University of Science and Technology Beijing, Beijing, 100083, People's Republic of China
[d] Department of Mechanical Engineering, University of South Florida, Tampa FL 33620, USA

ARTICLE INFO

Article history:
Received 6 January 2015
Received in revised form 7 April 2015
Accepted 7 April 2015
Available online 17 April 2015

Keywords:
Corrosion
Friction
Metal ion release
Surface modification
Wear mechanism.

ABSTRACT

CoCrMo alloy corrosion and tribocorrosion properties are crucial for orthopedic implant application. These properties have been enhanced by implanting nitrogen ions with 100 keV energy. The corrosion current density of the implanted alloy is reduced by an order of magnitude, compared with the original alloy without implantation. In the tribocorrosion tests, the potential of the implanted alloy remain almost unchanged at around 0.05 V versus Ag/AgCl, while the potential of the original alloy without implantation changes from −0.4 to −0.6 and then to about −0.5 V versus Ag/AgCl, showing typical tribocorrosion behavior. Tribocorrosion tests also show that the 4×10^{17} N^+/cm^2 implantation reduces the friction coefficient from 0.35 to 0.15. Various characterization results indicate that the implantation induces a novel composite microstructure of the nanocrystalline CrN embedded inside amorphous CoCrMo matrix in the implanted layer, which enhances hardness, corrosion and tribocorrosion properties.

© 2015 Elsevier B.V. All rights reserved.

1. Introduction

CoCrMo alloys have been used as orthopedic implant materials for more than 70 years due to their biocompatibility and beneficial combination of high strength and fatigue resistance, low creep, low to moderate elastic modulus, and high resistance to wear and corrosion [1,2]. However, once implanted in vivo, they perform under tribological contacts and loads, lubricated by the hostile corrosive body environment (biological fluids). Wear between the load bearing surfaces leads to the release of metal particles into the human body, while the biological corrosion causes the metal ions release (Co and Cr) from the CoCrMo alloy surface, along with the wear debris. Tribocorrosion causes CoCrMo alloy to degrade at a higher rate than corrosion alone. Over time, the accumulation of wear debris around the joint area could induce inflammation of the surrounding tissue and bone osteolysis at the bone-implant interface, resulting in the subsequent implant loosening. Meanwhile, the level of metal ions may become clinically significant, resulting in cytotoxicity, tissue necrosis and adverse immunological reactions, hypersensitivity [3,4] and ultimately the implant failure. Studies have revealed the toxic effects of metal ions released from the orthopedic implants [5], and the most toxic ions are Co and Cr [6].

Most published research papers dealing with the CoCrMo alloy orthopedic implants tribological behavior describe a characteristic wear pattern, which is initially accompanied by the large amount of wear debris during the running-in period, after which the wear rate decreases to a lower steady state value. Chistian [7] found that the released Co levels continuously increased during the running-in period and showed a significant decrease thereafter.

Two categories of the surface treatment have been considered for improving the wear and corrosion resistance of the CoCrMo alloys. One strategy is to thicken the protective oxide layer already present on the surface, which serves as a barrier in the alloy systems via hot concentrated nitric acid, or implantation with oxygen. The other strategy is to apply additional protective layers to act as a physical barrier between the bearing surfaces, such as coatings and ion implantation with different elements (C and N). However, producing consistent coatings that influence the physical and chemical behavior of the implant surface in the body is cumbersome, since coatings themselves present spalling and delamination problems [8]. The diffuse interface between the implanted layer and the unaffected material volume minimizes interfacial stresses, significantly reducing the likelihood of peeling.

* Corresponding author. Tel./fax: +86 10 82376048.
E-mail address: pangxl@mater.ustb.edu.cn (X. Pang).

http://dx.doi.org/10.1016/j.apsusc.2015.04.054
0169-4332/© 2015 Elsevier B.V. All rights reserved.

In the present work nitrogen ion implantation as means of forming a protective layer on the CoCrMo alloys surface was examined. Wettability and the corrosion resistance of the implanted layer were investigated, along with the ability of nitrogen implanted samples to resist metal wear loss and ion release caused by the interactive effects of wear and corrosion.

2. Materials and methods

2.1. CoCrMo alloy

The metal used in this study was medical grade CoCrMo alloy (ASTM F-75), with the composition given in Table 1. The test specimens in the form of discs, 20 mm in diameter and 5 mm thick were ground and polished on one side to the mirror-like finish with the mean surface roughness (R_a) of about 1.4 nm, based on the atomic force microscopy (AFM) results.

2.2. Nitrogen ion implantation

Samples were nitrogen ion implanted using a relatively simple ion implanter. As a preparation for ion implantation, the samples were initially cleaned ultrasonically in acetone and alcohol, and once in the ion implanter chamber, the samples were sputter cleaned with argon ions at 5 keV to remove residual surface contaminants. The surface modification process by nitrogen ion implantation was carried out at 100 keV at near-room temperature, which does not alter the alloy microstructure. The plasma was generated by the electron cyclotron resonance, and the plasma source was operated at 1000 W power and 2.45 GHz frequency. In order to evaluate the effect of different ion doses on the surface properties, five levels of the implantation dose of 1.5×10^{17}, 2.0×10^{17}, 2.5×10^{17}, 3.5×10^{17} and 4.0×10^{17} N^+/cm^2 were chosen.

2.3. Wettability

The wettability of the CoCrMo alloy before and after nitrogen implantation was measured using the sessile drop method by pouring 2 μL droplets of distilled water from the end of a syringe needle on the horizontal alloy surface. The cross section of the droplets was observed directly using an Olympus BX-41 optical microscope objective lens, and was digitally captured with a 1.4 megapixel computer-controlled CCD camera. The values reported here are average of more than 5 measurements performed in different areas of each sample surface. The sliding angle measurements were performed using a mechanical level goniometer.

2.4. Potentiodynamic polarization measurements

Electrochemical measurements were performed in a conventional three-electrode cell. The working electrode was embedded in a Teflon holder, sealing the gap between the working electrode and the silica gel holder in order to minimize the occurrence of crevices, with an area of 15.7 cm^2 exposed to the solution. The counter electrode was platinum filament. Potentials were measured against a saturated Ag/AgCl electrode. Prior to measurements, samples were allowed to stabilize under the open circuit conditions to reach a stable value of the corrosion potential. Potentiodynamic measurements were then performed at 1 mV/s scan rate, between −800 mV and 1800 mV. The electrolyte was newborn bovine serum.

Table 1
Chemical composition of the medical grade CoCrMo alloy.

Element	Co	Cr	Mo	Si	Mn	Ni	Fe	C
Wt.%	Bal.	26.5–30.0	4.5–7.0	≤1.0	≤1.0	≤2.5	≤1.0	≤0.35

2.5. Tribocorrosion test

Tribocorrosion behavior of materials was evaluated using the reciprocating tribocorrosion equipment, shown in Fig. 1. Integrated electrochemical tests were performed using a ball-on-plate reciprocating UMT-2 tribo-tester on the samples immersed in the newborn bovine serum (NBS). A silicon nitride ball (5 mm in diameter) was chosen as the counterpart, and all samples were used as plates. The upper surface of the samples was exposed to the electrolyte and the lower surface was insulated and electrically connected to a potentiostat. The three-electrode cell was employed, which is a standard and common method to evaluate the corrosion behavior. The three electrodes were the working electrode (the specimen), the reference electrode (Ag/AgCl electrode) and the counter electrode (platinum filament). The sliding wear tests, which conformed to the ASTMG133, were performed with the three-electrode cell, capable of in situ measurements. Tribocorrosion tests were performed at the open circuit potential. A load of 5 N was applied to the Si_3N_4 ball, corresponding to the Hertzian contact pressure of 928 MPa, calculated for the untreated samples. The sliding frequency was 1 Hz and the stroke length was 15 mm.

The tribocorrosion test consisted of the three steps: (1) stabilization of the open circuit potential (OCP) for 30 min; (2) rubbing under the open circuit potential for 4 h; (3) standby at the open circuit potential after rubbing for 30 min. At the end of the tests the samples and the balls were rinsed in distilled water and air-dried. After the tribocorrosion test, wear scar volume, wear morphology and concentrations of metal ions (Co and Cr) were examined.

2.6. Surface characterization

Auger electron spectroscopy (AES) was performed on the implanted sample (2.0×10^{17} N^+/cm^2) in the PHI 700Xi Auger system at a base pressure of 3×10^{-7} Pa. Depth profiling was conducted using 3 kV, 30 mA argon ion beam at 7 mPa pressure with 6 s sputter cycles. Standard SiO_2 was used to determine the sputtering rate of 69 nm/min. Atomic force microscopy was utilized to obtain the mean surface roughness, R_a (50×50 μm scan size) and the three-dimensional morphology (1×1 μm scan size). X-ray diffraction (XRD) was used to detect the near surface crystal structure at a scanning rate of 8°/min using grazing-incidence technique (GIXRD) to probe the implanted layer phases. The grazing angle was kept at 0.5° and 3° with CuK_α radiation ($\lambda = 1.5404$ Å) at a scanning rate of 3°/min. X-ray photoelectron spectroscopy (XPS) investigations were performed using AlK_α X-ray source (1486.6 eV). The binding energy was calibrated using the C1s peak at 284.8 eV.

Transmission electron microcopy (TEM, JEOL FasTEM) was used to examine the microstructure changes upon nitrogen ion implantation. Nano-hardness tester (N2100) was used for extracting surface hardness of the unimplanted and implanted samples as a function of the indentation depth. Optical microscopy was used for surface observations. Inductively coupled plasma mass spectrometer (ICP-MS) was used for measuring the concentrations of metal ions (Co and Cr) released into the simulated body fluid (NBS) during the tribocorrosion test. The solutions used by each tribocorrosion test were retrieved by pouring the cell content into the plastic container, then diluting it with 2 vol.% HNO_3. 2D profilometry was used for quantifying the volume of the wear tracks. The cross-section profiles were taken across the wear track for each sample at one-sixth, one-third, one-half, two-third and five-sixths of the wear track length. The total volume loss was obtained by

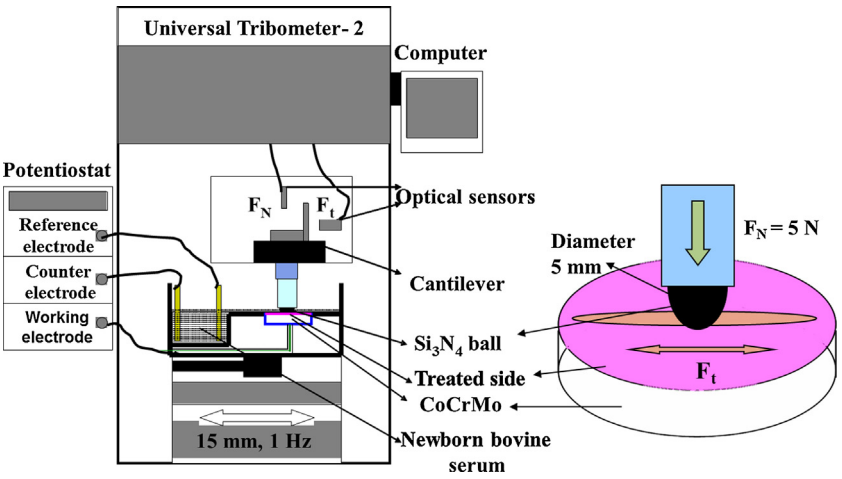

Fig. 1. Schematic representation of the tribocorrosion system.

multiplying the average area of the cross-sectional profiles by the wear track length.

3. Experimental results

3.1. Wettability

The contact angle values of water on the CoCrMo alloy surface before and after nitrogen ion implantation are shown in Fig. 2. It can be seen that after nitrogen ion implantation, the contact angle increased from 70.1° to >90° and water wettability changed from hydrophilic to hydrophobic. However, the contact angle did not change much with the different implantation dosage. The contact angle is affected by the surface morphology. The implanted CoCrMo alloy surface presents the bubbling shape structure caused by the ion bombardment and sputtering effects of ion implantation. Based on the study of nearly 300 kinds of plant leaf surfaces, Barthlott concluded that their self-cleaning ability (hydrophobicity) is determined by the rough surface, the pulvinus and the mastoid microstructure, called "the lotus leaf effect" [9].

3.2. Corrosion results

Potentiodynamic polarization curves were recorded in the newborn bovine serum during static tests for all samples, shown in

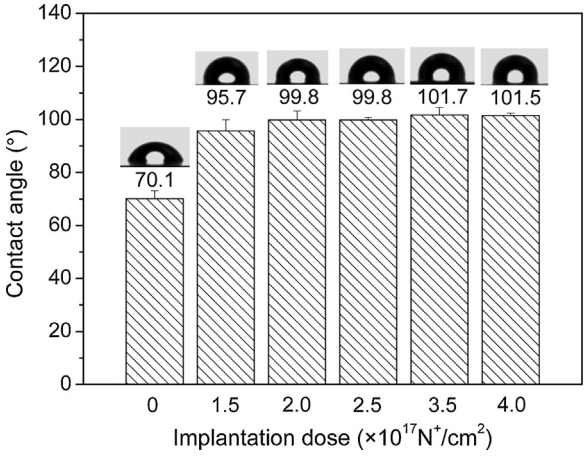

Fig. 2. Water contact angle on the surface of the CoCrMo alloy before and after nitrogen ion implantation.

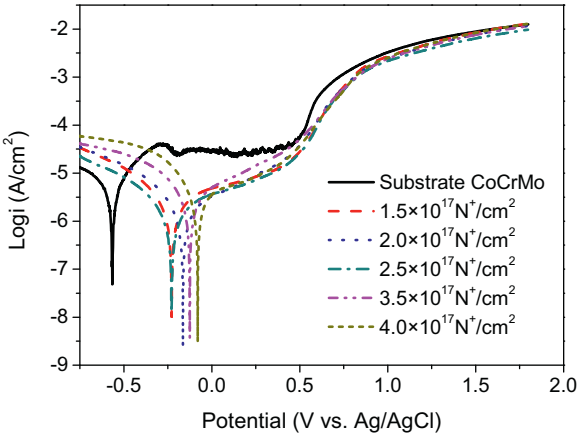

Fig. 3. Polarization curves of the unimplanted CoCrMo alloy (the substrate material) and the specimens implanted with nitrogen at different doses of 1.5×10^{17}, 2.0×10^{17}, 2.5×10^{17}, 3.5×10^{17} and 4.0×10^{17} N$^+$/cm^2 in the newborn bovine serum.

Fig. 3. The shape of the curves is similar, although there are several important differences. The ion implantation increased the open circuit potential with the injection dosage, with respect to the untreated CoCrMo alloy. However, this is only the first approximation of the material behavior, and other parameters, like the corrosion current and polarization resistance must be taken into account in order to evaluate corrosion kinetics. The corrosion current density values and the polarization resistance extracted from the polarization curve are shown in Fig. 4(a) and (b), respectively. There is no clear relation between the R_p values, current density and the implantation dose. For the injection dose less than 3.5×10^{17} N$^+$/cm^2, the value of the corrosion current gradually reduced and the polarization resistance gradually increased. However, with the injection dose increasing beyond 3.5×10^{17} N$^+$/cm^2, the current density increased and the polarization resistance decreased. Therefore, higher injection doses reduce the alloy corrosion resistance. An increase in the open circuit potentials values, R_p, and a decrease in the current density co-determine improved corrosion protective properties. In the static corrosion test different implantation doses caused varying corrosion resistance performance, and the sample implanted with the 2.5×10^{17} N$^+$/cm^2 dose presents the best corrosion resistance.

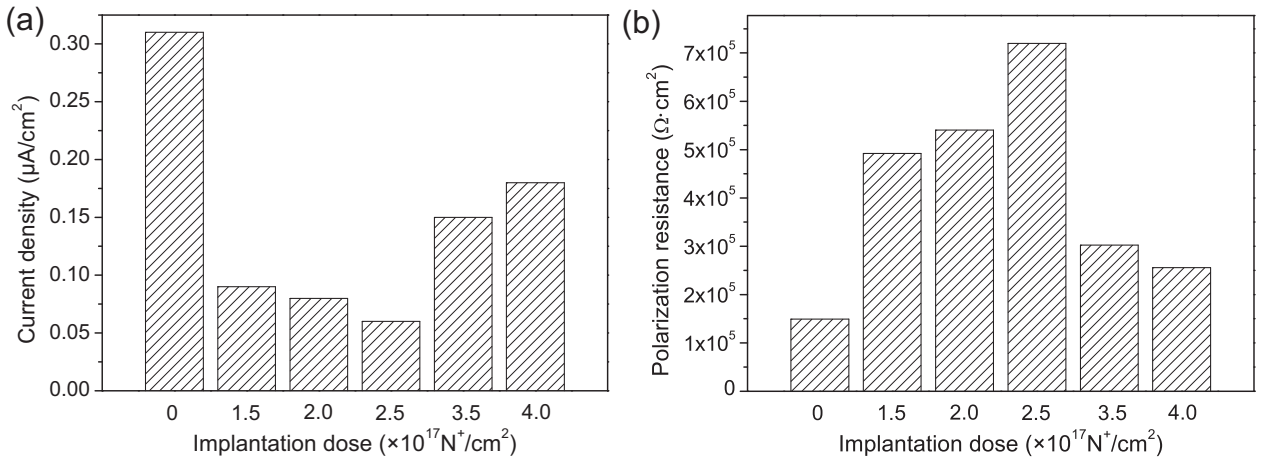

Fig. 4. (a) Corrosion current and (b) polarization resistance variation with the implantation dose.

3.3. Tribocorrosion results

3.3.1. Friction coefficient and OCP

Fig. 5(a) shows the evolution of the open circuit potential prior, during and after the wear tests, where three regions can be clearly seen. Region 1 is before the wear test onset, and different OCPs of the alloy surface in NBS are clearly apparent for the untreated sample and those implanted with different nitrogen ion doses. Once the wear starts (ball reciprocation), the potential instantaneously decreases, corresponding to the surface oxide film damage (depassivation). Within region 2, the potential finally maintains at a relatively constant level, where an active-passive cell between the wear scar and the surrounding passive surface is established. In region 3, the potential recovery corresponds to the film passivation. However, the samples with the 1.5×10^{17}, 2.0×10^{17} and 2.5×10^{17} N^+/cm^2 doses showed a sharp potential decrease during sliding, after approximately 1500 s from the wear onset. This transition is attributed to the modified layer damage, leading to the substrate material exposure to the solution. However, potential of the N 3.5×10^{17} and 4.0×10^{17} N^+/cm^2 samples shows no sharp decrease, indicating no substrate material exposure. During the tribocorrosion tests, the potential of the nitrogen ion implanted CoCrMo samples is higher than the untreated samples, and increases with the injection dose.

Fig. 5(b) shows the coefficient of friction evolution with time during the tribocorrosion tests (reciprocating ball-on-plate) performed at the open circuit potential for all CoCrMo alloy samples (un-implanted and nitrogen ion implanted samples with different doses of 1.5×10^{17}, 2.0×10^{17}, 2.5×10^{17}, 3.5×10^{17} and 4.0×10^{17} N^+/cm^2). Obviously the friction coefficient decreased with the implantation dosage. The untreated alloy showed a constant value of approximately 0.34 for the entire test duration. Samples with 1.5×10^{17}, 2.0×10^{17} and 2.5×10^{17} N^+/cm^2 presented a similar sharp change, corresponding with the electrochemical parameters transition, recorded after approximately 1500 s from the sliding onset.

3.3.2. Wear results

The wear track profiles measured by the two-dimensional profilometry of the worn samples and the corresponding wear track volume are shown in Fig. 6. The net reduction in the wear damage of the implanted samples, compared with the untreated alloy, can be directly seen. The effect is more pronounced with the increasing nitrogen ion implantation dose. The injection doses of 3.5×10^{17} N^+/cm^2, or 4.0×10^{17} N^+/cm^2 cause a 100 fold wear resistance increase.

Fig. 7 shows the worn surface morphology of the untreated and nitrogen ion implanted CoCrMo alloy. It is clear that the worn surfaces of the untreated CoCrMo alloy samples under tribocorrosion show plastic deformation and sharp plough grooves. After implantation, the worn surfaces exhibit shallower, relatively smooth grooves and fewer abrasion pits. Higher nitrogen ion implantation

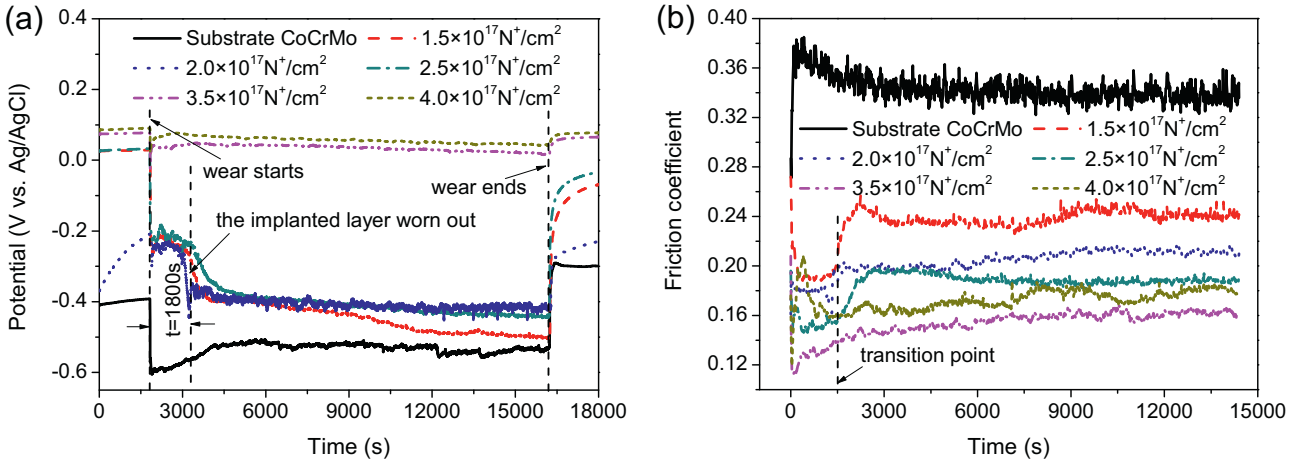

Fig. 5. (a) Potential and (b) friction coefficient evolution with time during the tribocorrosion tests in newborn bovine serum at the open circuit potential of unimplanted and nitrogen ion implanted samples with different doses of 1.5×10^{17}, 2.0×10^{17}, 2.5×10^{17}, 3.5×10^{17} and 4.0×10^{17} N^+/cm^2.

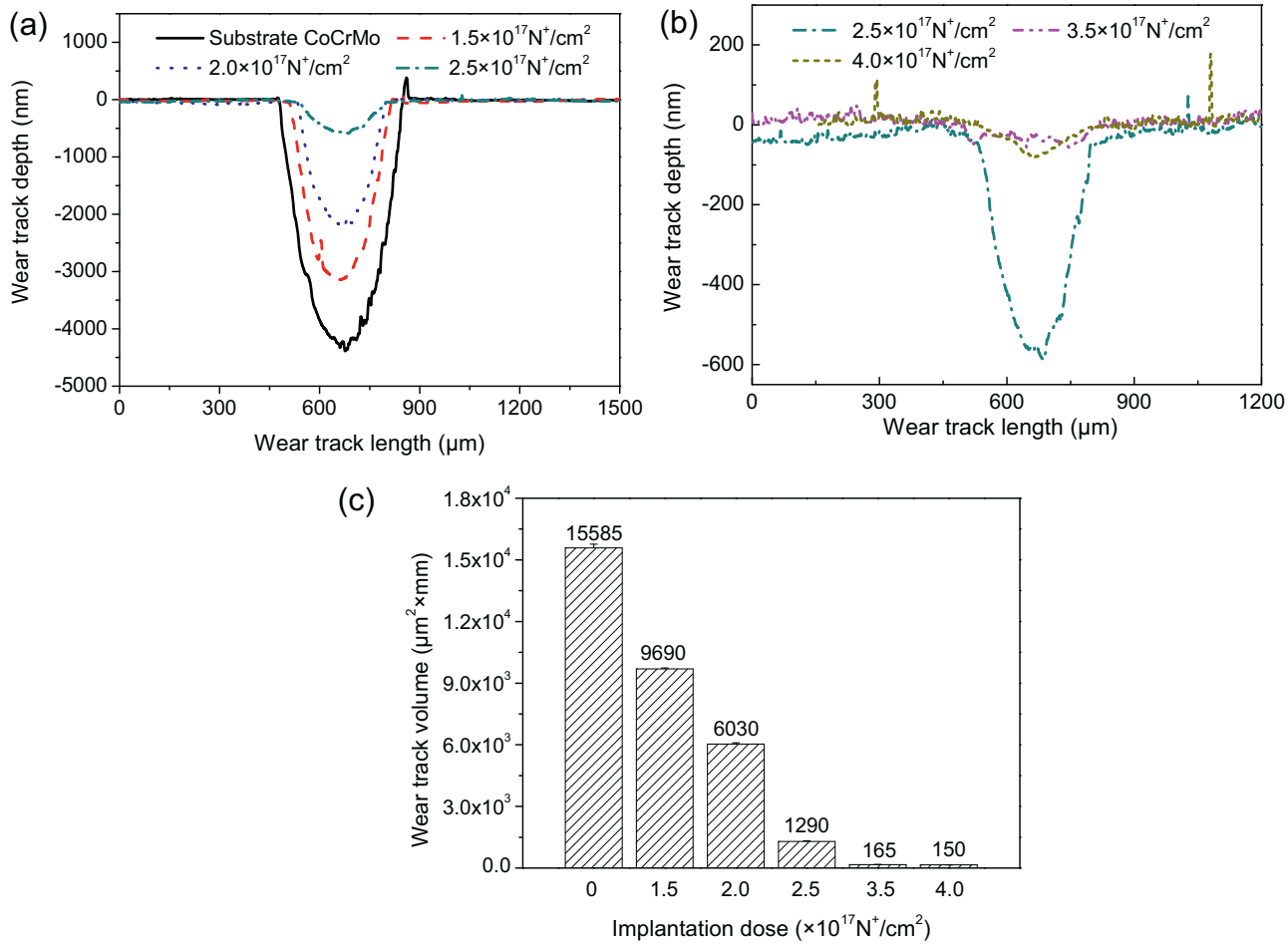

Fig. 6. (a) and (b) Wear track cross-section profiles and (c) the wear track volume of untreated and nitrogen ion implanted CoCrMo alloy under the 5 N normal load.

leads to shallower plough grooves. Fig. 8(a) shows the wear damage of a silicon nitride ball as the counterpart after 4 h wearing. There is a little wear damage with plough grooves and abrasion pits on the surface of the ball. Fig. 8(b) shows the profiles of the ball before and after 4 h wearing. One can see the wearing depth is about 4 μm maximum.

3.3.3. Ion concentration effects

CoCrMo samples before and after nitrogen ion implantation were compared using corrosion resistance tests under wear (tribocorrosion tests) in NBS. Using ICP-MS, the concentration of Co and Cr ions released into the NBS fluid from the specimens was determined, shown in Fig. 9. For all samples, the concentration of released cobalt ions is greater than the concentration of chromium ions. The corrosion of CoCrMo alloys in NBS solution happens primarily by selective cobalt dissolution. Co and Cr ion release rates initially increase with nitrogen ion implantation dosage. The maximum Co and Cr ions concentration is observed for the N 2.0×10^{17} N^+/cm^2 sample. Subsequently, the concentration of the released ions goes down to a level lower than the concentration of the Co and Cr ions released from the CoCrMo alloy substrate.

3.4. AES

The elemental depth profiles of implanted CoCrMo with the dose of 2.0×10^{17} N^+/cm^2 using AES are shown in Fig. 10. Depth profiles of Co, Cr, Mo and N in the near-surface layer were analyzed. It is clearly seen from Fig. 10 that N profiles in the implanted CoCrMo alloy show non-Gaussian distribution. The migration of N atoms to the surface is revealed with a slight increase of N concentration near the surface. An alternative mechanism might be radiation-induced segregation, where interstitial solute N atoms are carried by the defect flux moving towards the surface [10]. The strong bonds formed between the implanted N atoms and the substrate Cr and Mo atoms render implanted N relatively immobile, despite the concentration gradients, the stress and the defect flux, all of which could drive N atoms to the surface [11]. The maximum N concentration occurs at a depth of about 15 nm. Moreover, from the sharp decrease of Cr and Mo concentrations, and the sharp increase of Co content near the top 15 nm of the surface, it can be assumed that the affinity of Cr and Mo to N is grater than the affinity of Co to N.

3.5. AFM

AFM was used to study the CoCrMo alloy surface modification caused by ion implantation. Two-dimensional morphology (50×50 μm scan size, mean roughness calculated from the 2D-morphology) of the implanted and un-implanted samples are shown in Fig. 11(a) and (b) (representative AFM data for the 2.0×10^{17} N^+/cm^2 dose). The ion implantation causes a rougher surface. Surface roughness of the untreated samples is about 1.4 nm. Surface roughness of the as-treated samples is between 3 nm and 3.7 nm. Meanwhile, grains with clear boundaries begin to emerge after implantation, resulting from the etching effect of ion

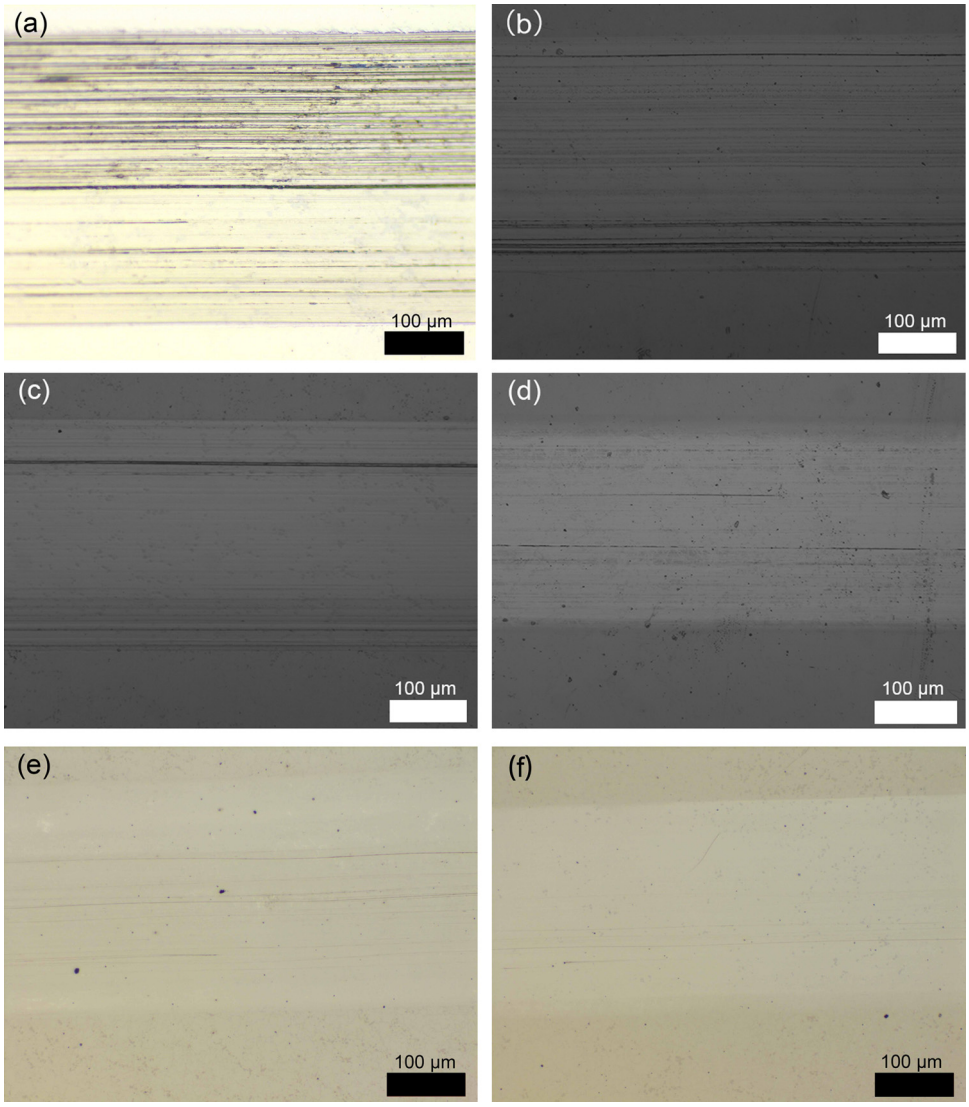

Fig. 7. Morphology of the worn surfaces of: (a) CoCrMo alloy substrate, (b) 1.5×10^{17}, (c) 2.0×10^{17}, (d) 2.5×10^{17}, (e) 3.5×10^{17} and (f) 4.0×10^{17} N^+/cm^2.

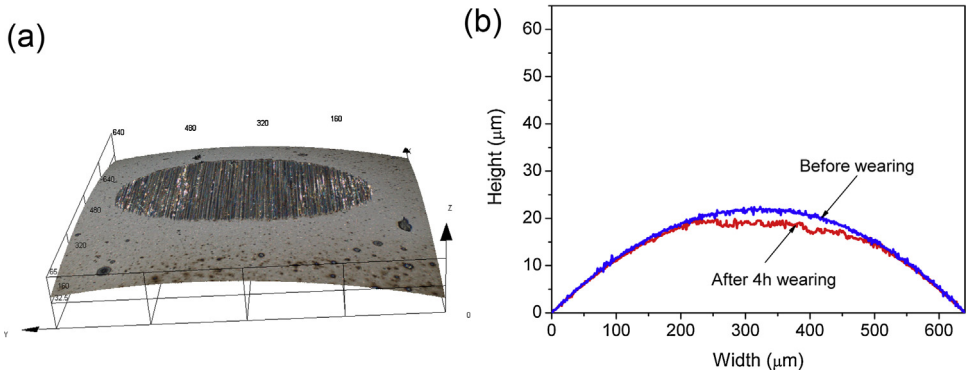

Fig. 8. The wear damage of a silicon nitride ball as the counterpart (a) morphology of the worn surface after 4 h wearing, (b) the profiles of the ball before and after 4 h wearing.

implantation. From the three-dimensional morphology (1×1 μm scan size), shown in Fig. 11(c and d), the scratches caused by polishing become shallow, and at the same time the bubbling shape appears due to the ion bombardment and sputtering effects of ion implantation.

3.6. XRD and GIXRD

Fig. 12 shows the $\theta/2\theta$ XRD (Bragg-Brentano geometry) results for the implanted and un-implanted specimens. The effective XRD probe depth is 1–6 μm, obtained from $\sin\theta/2$ μ [12]. The CoCrMo

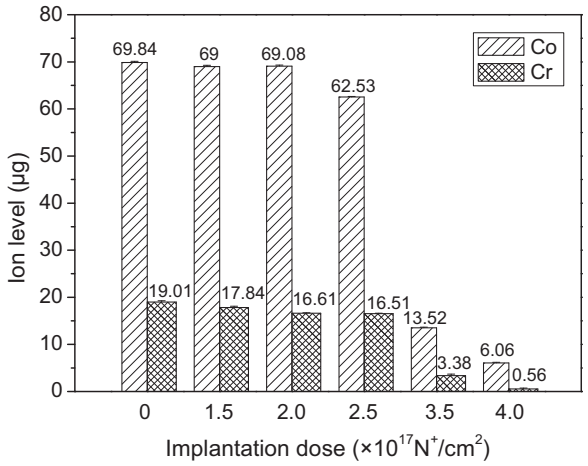

Fig. 9. Co and Cr ions concentrations released into the simulated body fluid (newborn bovine serum) during the tribocorrosion test measured by ICP-MS.

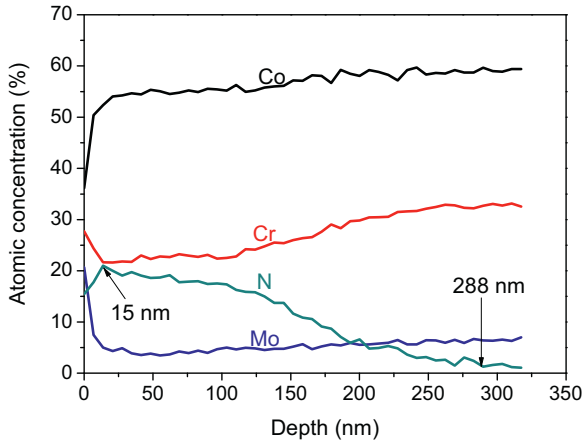

Fig. 10. AES elemental depth profiles after CoCrMo alloy nitrogen ion implantation at the 2.0×10^{17} N^+/cm^2 dose.

alloy substrate is made up of fcc γ-(Co,Cr,Mo) and hcp ε-(Co,Cr,Mo). From Fig. 12, it is clear that the intensity of hcp ε-(Co,Cr,Mo) is gradually weakened, until it disappeared with the increasing implantation dose. However, the presence of the implanted layer is not apparent in the XRD results, probably due to the higher intensity substrate signal.

To reveal the N implanted layer phases at the near surface, grazing incidence X-ray diffraction (GIXRD) of the same samples was carried out at the incident angle of 0.5°, and the results are shown in Fig. 13(a)–(b). The square root intensity in Fig. 13(b) and (c) was used to visually enhance the weaker peaks. The effective depth probed by Cu-Kα X-ray beam at the 0.5° incident angle was about 34 nm, according to the relationship between the detection depth and the incident angle: $\sin(\Psi/\mu)$ [12]. An important observation is the interstitial phase formation (nitrogen occupying octahedral sites of the fcc lattice in the supersaturated phase), γ_N phase formation (the expanded structure of the γ phase) is similar to that observed for the pulsed plasma nitrided [13] and nitrogen ion implanted CoCrMo orthopedic implant materials [14]. For the 1.5×10^{17} N^+/cm^2 dose, the near-surface (34 nm) is mainly composed of the γ_N and CrN phases (inferred from the broad peak at $2\theta = 42.9°$, the decreasing intensity of the γ_N phase, confirmed by subsequent XPS results), where the fcc γ-(Co,Cr,Mo) and the hcp ε-(Co,Cr,Mo) phases disappear. With the increasing implantation dose, the content of the γ_N phase decreases and the CrN phase scales up. This may be induced by the decomposition of Cr

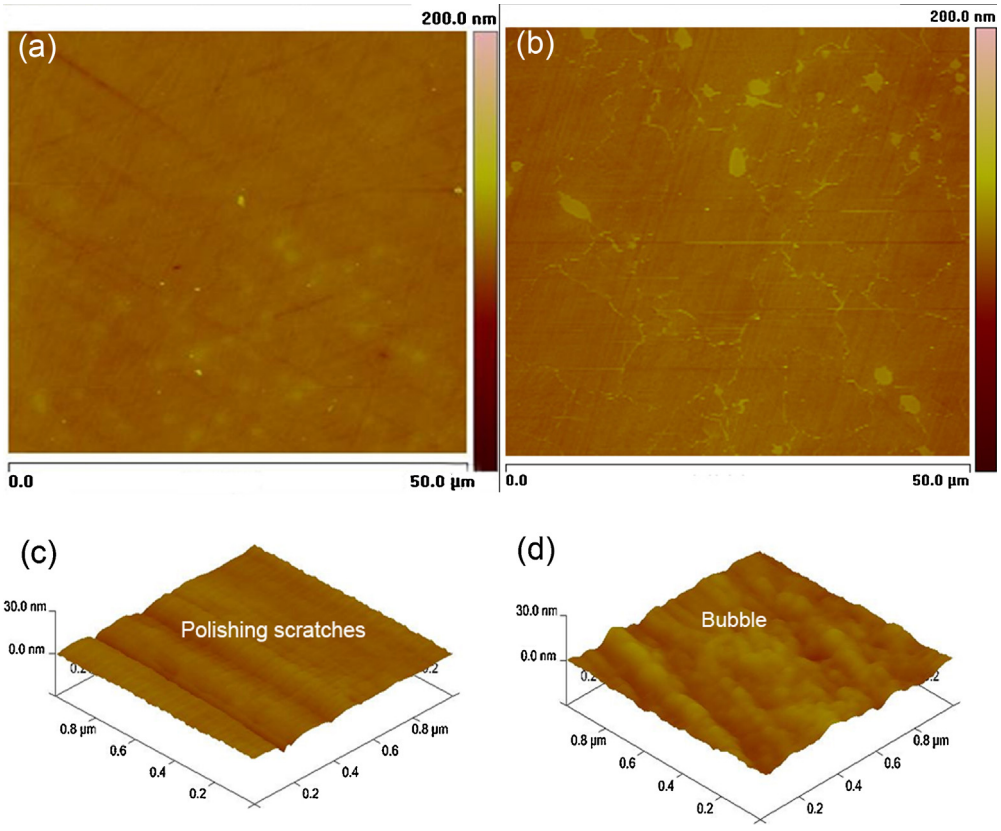

Fig. 11. Two-dimensional and three-dimensional AFM images of the sample surface: (a), (c) unimplanted and (b), (d) implanted with a dose of 2.0×10^{17} N^+/cm^2.

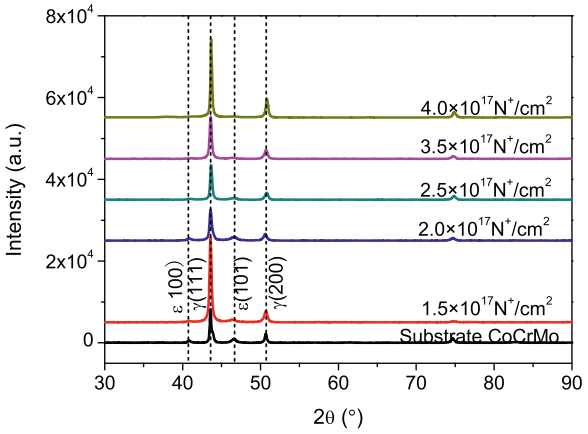

Fig. 12. XRD data of the unimplanted CoCrMo alloy (the substrate material) and the specimens implanted with nitrogen at different doses of 1.5×10^{17}, 2.0×10^{17}, 2.5×10^{17}, 3.5×10^{17} and 4.0×10^{17} N^+/cm^2.

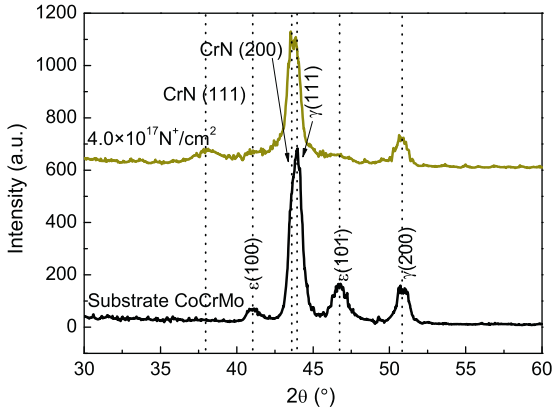

Fig. 14. GIXRD data (3° incidence angle) for the specimens unimplanted (the substrate material) and implanted with a dose of 4.0×10^{17} N^+/cm^2.

from the metal matrix phase [15]. The effect increases with greater implanted ion dosage. The γ_N phase disappears at the injection dose of 2.5×10^{17} N^+/cm^2, while the peak of the CrN phase becomes broader, indicating the formation of the amorphous and nanocrystalline phases. Until the injection dose of 4.0×10^{17} N^+/cm^2 is reached, no obvious peaks are seen. Whether the nanocrystalline and amorphous phases cause diffraction peak widening, can be examined by TEM microstructure characterization before and after nitrogen ion implantation. In order to evaluate the phase change beyond 34 nm, the grazing angle of 3° was used for the implantation dose of 4.0×10^{17} N^+/cm^2, shown in Fig. 14. Besides the matrix γ phase, another peak appears, labeled as the CrN (200) phase. The CrN (1 1 1) reflection is also present.

3.7. XPS

Fig. 15 presents the Cr2p3/2, Co2p, Mo3d5/2 and N1s spectra of the CoCrMo alloy before and after nitrogen ion implantation at a dose of 4.0×10^{17} N^+/cm^2. In all cases, a decreasing metal signal is observed after implantation, indicating the protective oxide layer formation. In the case of Cr and N, formation of the CrN phase after ion implantation is demonstrated, in agreement with the XRD results.

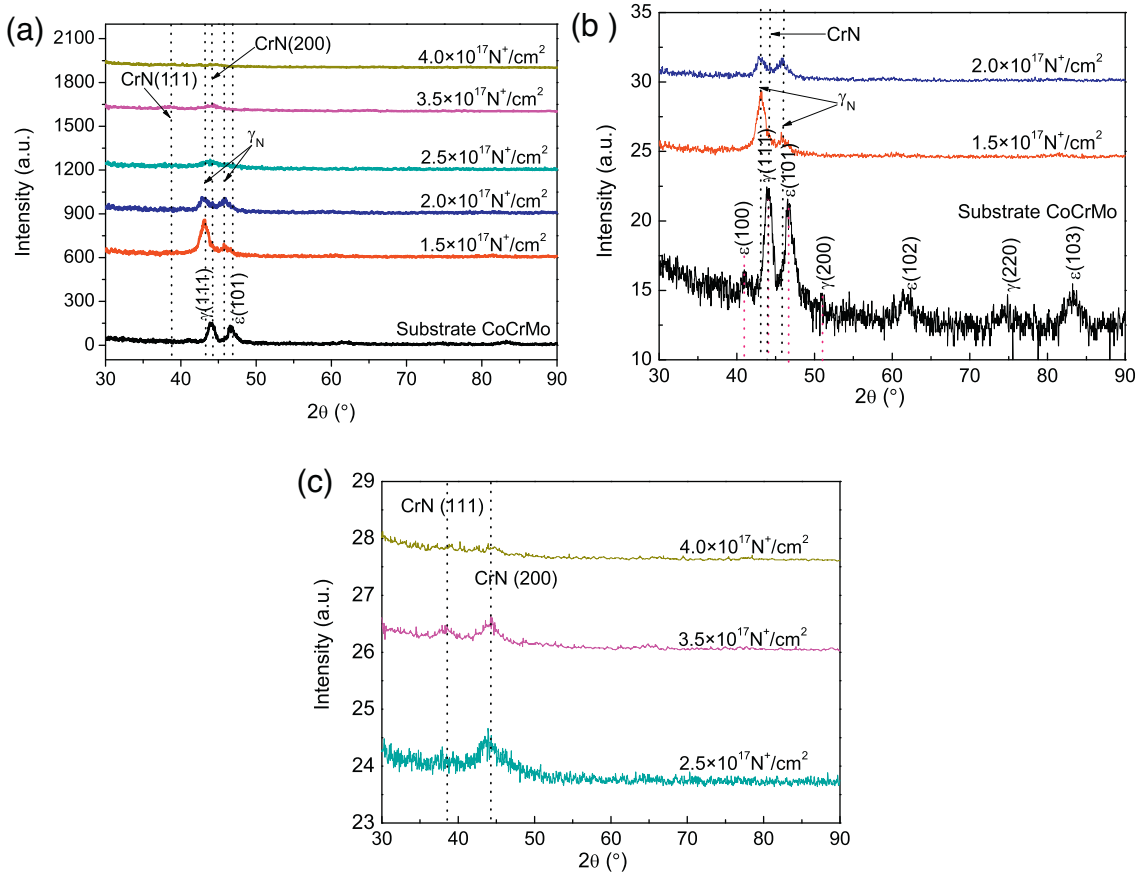

Fig. 13. GIXRD data (0.5° incidence angle) of the specimens nitrogen implanted at different doses of 1.5×10^{17}, 2.0×10^{17}, 2.5×10^{17}, 3.5×10^{17} and 4.0×10^{17} N^+/cm^2 (a); the square root intensity is used to visually enhance the weaker peaks (b) and (c).

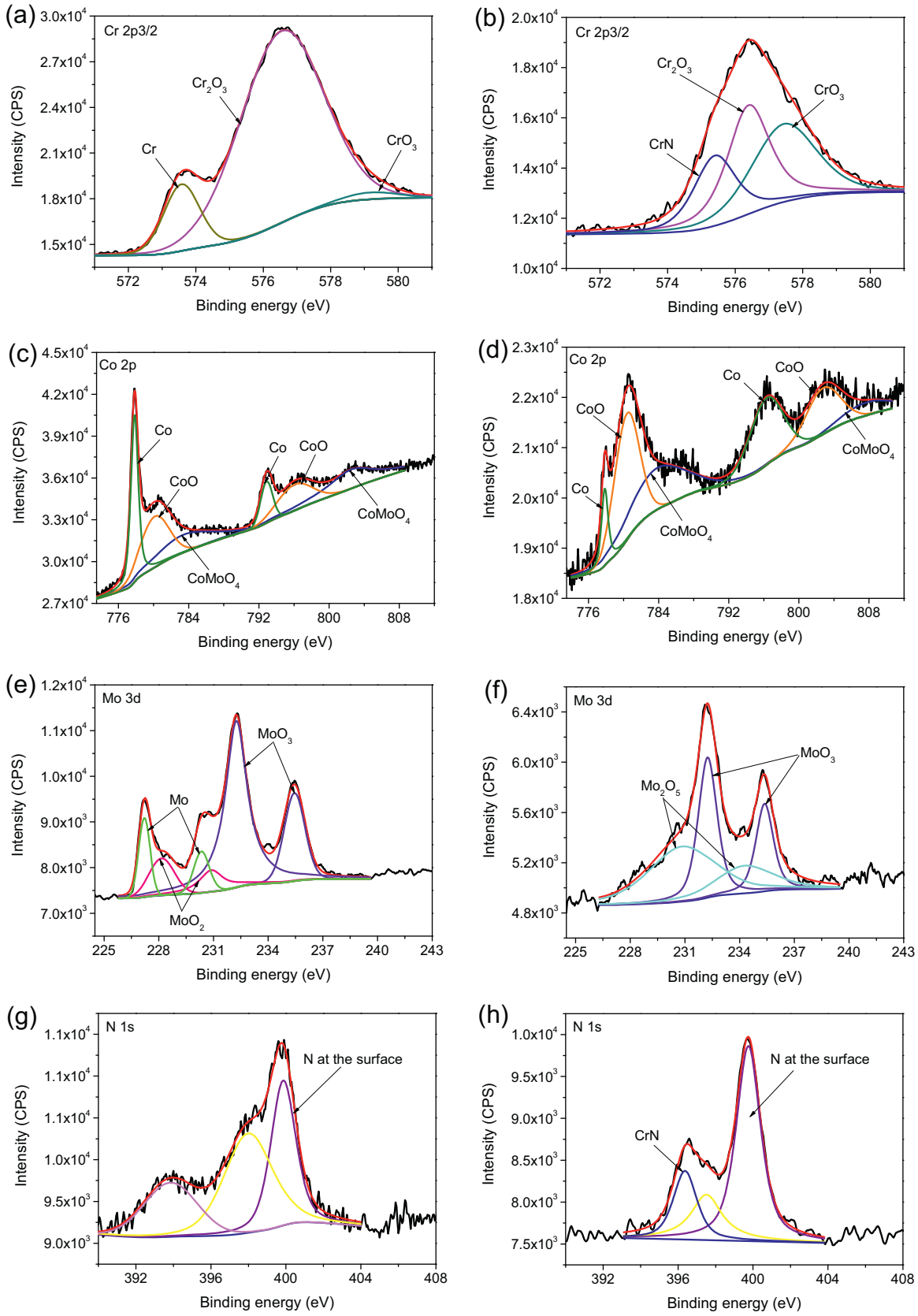

Fig. 15. Examples of fitted XPS spectra for CoCrMo before (a), (c), (e), (g) and after (b), (d), (f), (h) nitrogen ion implantation.

3.8. TEM

Fig. 16 shows high resolution TEM images (representing the whole surface microstructure) before and after nitrogen ion implantation at a dose of 2.5×10^{17} N^+/cm^2, respectively. The CoCrMo alloy substrate mainly consists of the fcc-austenite and twin hcp-martensite (seen in Fig. 16(b)). In Fig. 16(d) the twin hcp-martensite disappeared, and the majority of the implanted layer surface appears amorphous with nanocrystalline CrN embedded in the amorphous surface.

3.9. Nanoindentation hardness

Nanoindentation is a useful technique to characterize the surface and subsurface mechanical properties of materials. Using dynamic loading, the hardness change with the indentation depth was obtained in Fig. 17. The hardness value is an average of 10 measurements. The hardness of implanted CoCrMo alloy is higher than the untreated specimens. The hardness increases with the injection dose. This can be attributed to the presence of compressive residual stresses and the formation of harder phases (CrN) in the implanted sample. Increasing hardness of the ion implanted materials has been observed earlier [16]. The solute nitrogen ingresses the crystal lattice to form a metastable phase (γ_N and CrN phases), which hinders the dislocation movement [17] and contributes to the hardness increase after ion implantation. Moreover, the similarity of the N depth profiles and hardness indicates that the dislocations induced by implantation can also cause the hardness increase [18]. The hardness of the implanted CoCrMo near the surface is lower than the CoCrMo substrate.

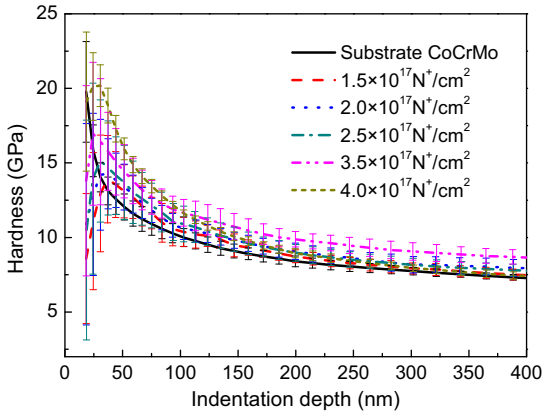

Fig. 17. Nanoindentation hardness of unimplanted and implanted samples with the dose of 1.5×10^{17}, 2.0×10^{17}, 2.5×10^{17}, 3.5×10^{17} and 4.0×10^{17} N^+/cm^2.

4. Discussion

Nitrogen ion implantation has been successfully applied to metallic biomaterials [19]. When high energy nitrogen ions interact with the CoCrMo alloy surface, they cause surface atoms displacement and defects due to the sputtering effect. At the same time, the momentum from the nitrogen ions is passed to the atoms below. Due to preferential sputtering, the atoms gain less momentum prior to the surface segregation. Based on the AES profile results, the concentration of Cr and Mo at the surface is higher than near the surface due to the surface segregation. The energy of nitrogen atoms is reduced at the near-surface, forming a barrier layer. Consequent nitrogen atoms diffused at a slower rate, rendering the depth

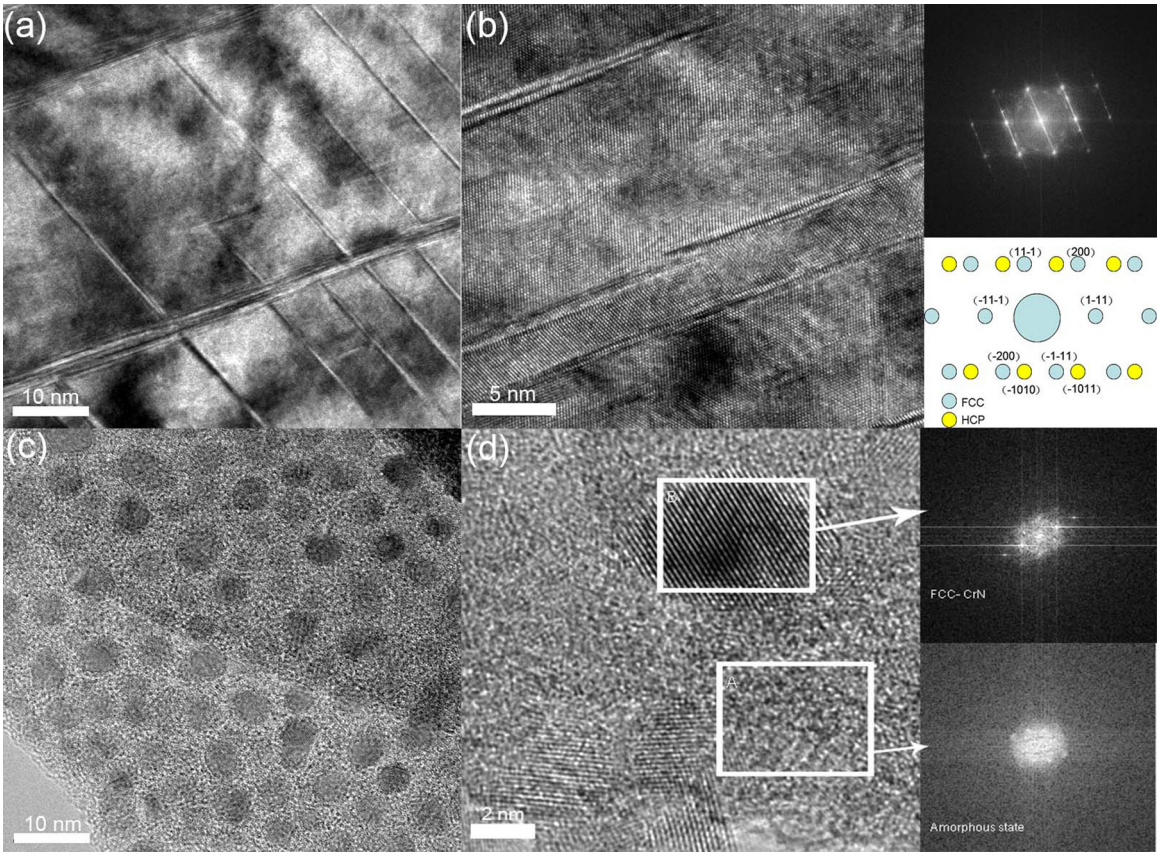

Fig. 16. High-resolution TEM images of the CoCrMo alloy before (a), (b) and after (c), (d) nitrogen ion implantation at a dose of 2.5×10^{17} N^+/cm^2.

profile in Fig. 9. XRD results revealed the expanded γ_N phase, CrN phase and the amorphous phase. XPS results also confirmed the CrN phase presence, along with TEM, which also revealed the CrN phase generation after nitrogen ion implantation.

At low injection dose, the implanted N remains in the solid solution (fcc phase), generating the so-called expanded γ_N phase (seen from the 1.5×10^{17} N^+/cm^2 XRD results). When the solubility limit is exceeded at higher injection dose, the precipitation of Cr nitrides occurs [20]. Based on the 1.5×10^{17} N^+/cm^2 XRD results, both γ_N and CrN phases appeared, however, since the CrN phase was not obvious, the XPS results of the 2.0×10^{17} N^+/cm^2 sample proved that the CrN phase was indeed produced. The γ_N phase is a metastable phase with stored energy, which can be used for transformation of the surface microstructure during the friction test to optimize the surface tribological properties [21]. CrN precipitation produces high stress, concentrated in the surface layer, causing accumulation of the residual stress, which can improve the wear resistance and hardness [22]. Meanwhile, the CrN phase can also act as a pinning source for dislocation movement and lead to wear resistance and hardness enhancement [23].

TEM results of the 2.5×10^{17} N^+/cm^2 sample revealed the occurrence of the nanocrystalline CrN. The proportion of the nanocrystalline structure increased gradually with the higher implantation dose. Meanwhile, the increasing amount of the nanocrystalline phase further contributes to the XRD peak broadening. It is known that amorphous alloys containing corrosion-resistant elements showed higher corrosion resistance than fully crystallized alloys with the same composition. Amorphous alloys are metastable and hence surface reactivity is high. High reactivity of an alloy surface leads to rapid dissolution of unnecessary alloying constituents, assisting the fast and significantly enriched chromium species to form a stable and highly protective passive film. However this is not always true when nanocrystalline phases are precipitated in the amorphous matrix. There are examples of the nanocrystalline phase precipitation in the amorphous matrix, which is detrimental in terms of corrosion [24]. However, the nanocrystalline phase appearance will introduce another reinforcement mechanism – fine grain strengthening, improving the alloy hardness. With the hardness increasing with ion implantation, the wear resistance increased because the wear mass loss is inversely proportional to the metal's hardness [25]. Additionally, high injection dose can increase the implanted layer damage, reducing the density of the injection layer and thus reducing the corrosion resistance [26].

Higher degree of noncrystallinity leads to higher corrosion resistance of the alloy. Meanwhile, nanocrystalline phase precipitation in the amorphous matrix will decrease the corrosion resistance of the alloy. Better corrosion resistance at the 2.5×10^{17} N^+/cm^2 dose may be due to the higher degree of amorphization, compared with the higher implantation dose.

Possible causes for hardness increase after ion implantation can be ascribed to the implantation-induced dislocations, compressive residual stresses, and the formation of the metastable γ_N phase, CrN precipitation, amorphous structure and the nanocrystalline phase, which combined lead to the hardness increase after injection at five different doses.

Combining XRD and hardness results, the increase of the alloys' hardness was mainly due to the formation of the CrN phase. As seen in the AFM images, the polishing marks disappeared, and bubbling shape structure appeared on the surface due to the ion bombardment and sputtering effect of ion implantation. The emerging bubbling structure on the surface after implantation caused the material change from hydrophilic to hydrophobic. The quantity of absorbed protein on the surface increased with the hydrophobic properties improvement [27]. Protein adsorption on the hydrophobic surface occurred due to dehydration or rearrangement reactions causing the entropy change [28]. The presence of protein in the metal-on-metal articular interface has the potential to form a boundary lubrication layer, or tribofilm, which effectively reduced the specimen surface damage [29,30]. The more protein absorbed on the surface, the less damage was caused by wear in the protein-rich solution. Too much protein adsorption on the surface may be one of the reasons for the decreased wear rate after injection.

The quantity of ions released also indicates the alloy corrosion resistance. The opposite results of the corrosion resistance from the static and trobocorrosion tests reflect no correlation between the static corrosion and the corrosion in friction tests [31]. The improvement in the wear resistance and friction coefficient is associated with materials surface hardness (nitrogen present in the CoCrMo matrix interstitial positions and precipitation hardening). However, the wear loss reduced significantly by 100 fold, as seen from the XRD, hardness and wear results for the 3.5×10^{17} N^+/cm^2 dose. Thus, the nanocrystalline CrN phase can greatly improve the alloy wear resistance.

From the tribocorrosion tests (wear track volume and released ion concentration), it is found that the reduction in the degree of ion release is not proportional to the reduction of the wear volume, compared with the CoCrMo alloy substrate. Therefore the metal ion release is mainly from the friction contact area and the wear-induced debris. Therefore, these results provide a strong evidence for the effect of the ion implantation process (ion dosage) on improving the corrosion and tribocorrosion performance of the CoCrMo alloy.

5. Conclusions

As nitrogen ions were implanted into the CoCrMo alloys, the hcp-CoCrMo phase at the near surface disappeared. The supersaturated solid solution of nitrogen in the fcc-CoCrMo (γ_N phase) was formed firstly, and then the CrN phase precipitated. With a higher nitrogen dose, the amount of CrN increased and the amount of the γ_N phase decreased. Exclusively amorphous layer appeared at the near surface with the injection doses between 2.0×10^{17} and 2.5×10^{17} N^+/cm^2.

The wettability of the material changed from hydrophilic to hydrophobic after nitrogen ion implantation. It has shown that nitrogen ion implantation could improve the corrosion resistance of CoCrMo alloy. The implanted specimens showed variations in the corrosion resistance with varying doses, and the specimen implanted with the dose of 2.5×10^{17} N^+/cm^2 showed an optimal corrosion resistance. The detrimental effect of the specimen implanted at higher doses was attributed to the formation of the nanocrystals in the amorphous matrix. In addition, it can be obtained that hardness increased with the increased implantation dose.

Acknowledgements

This work was supported by the Hong Kong scholar project and the National Nature Science Foundation of China (51001013, 51271022), Fok Ying Tung Education Foundation (132001) and the Fundamental Research Funds for the Central Universities. Authors thank Mr. Yusheng Yang at the Hong Kong University of Science and Technology for the TEM sample preparation and characterization.

References

[1] M. Long, H.J. Rack, Titanium alloys in total joint replacement—a materials science perspective, Biomaterials 19 (1998) 1621–1639.
[2] J.A. Disegi, R.L. Kennedy, R. Pilliar, Cobalt-Base Alloys for Biomedical Applications, ASTM STP 1365, Virginia, 1999.
[3] J.J. Jacobs, A.K. Skipor, L.M. Patterson, N.J. Hallab, W.G. Paprosky, J. Black, et al., Metal release in patients who have had a primary total hip arthroplasty.

Aprospective, controlled, longitudinal study, J. Bone Joint Surg. Am. 80 (1998) 1447–1458.
[4] T. Visuri, M. Koskenvuo, Cancer risk after Mckee-Farrar total hip replacement, Orthopedics 14 (1991) 137–142.
[5] Y. Okazaki, E. Gotoh, Comparison of metal release from various metallic biomaterials in vitro, Biomaterials 26 (2005) 11–21.
[6] M.G. Shettlermore, K.J. Bundy, Examination of in vivo influences on bioluminescent microbial assessment of corrosion product toxicity, Biomaterials 22 (2001) 2215–2228.
[7] C. Heisel, N. Streich, M. Krachler, E. Jakubowitz, J.P. Kretzer, Characterization of the running-in period in total hip resurfacing arthroplasty: an in vivo and in vitro metal ion analysis, J. Bone Joint Surg. Am. 3 (2008) 125–133.
[8] R. Venugopalan, J.J. Weimer, M.A. George, L.C. Lucas, The effect of nitrogen diffusion hardening on the surface chemistry and scratch resistance of Ti-6Al-4V alloy, Biomaterials 21 (2000) 1669–1677.
[9] W. Bartholtt, C. Neinhuis, Purity of the sacred lotus, or escape from contamination in biological surfaces, Planta 1 (1997) 1–8.
[10] A.D. Marwick, in: J.M. Poate, G. Foti, D.C. Jacobson (Eds.), Surface Modification and Alloying by Laser, Ion, and Electron Beams, Plenum, New York, 1983, p. 211.
[11] G. Dearnley, Stress-induced effects in sputtering and surface analysis, Appl. Phys. Lett. 28 (1976) 244–245.
[12] B.D. Cullity, Elements of X-Ray Diffraction, Adidison Wesley Publishing Company Inc, 1978, pp. 138.
[13] A. Bazzoni, S. Mischler, N. Espallargas, Tribocorrosion of pulsed plasma-nitrided CoCrMo implant alloy, Tribol. Lett. 49 (2013) 157–167.
[14] O. Öztürk, U. Türkan, A.E. Eroğlu, Metal ion release from nitrogen ion implanted CoCrMo orthopedic implant material, Surf. Coat. Technol. 200 (2006) 5687–5697.
[15] Bruce R Lanning, Wei Ronghua, High intensity plasma ion nitriding of orthopedic materials: Part II microstructure analysis, Surf. Coat. Technol. 186 (2004) 314–319.
[16] A.O. Olofinjana, Z. Chen, J.M. Bell, Ultra-high surface hardness in nitrogen ion implanted low alloy steel, Mater. Lett. 53 (2002) 385–391.
[17] A.O. Olofinjana, Z. Chen, J.M. Bell, Tribological properties of nitrogen ion implanted steel, Mater. Lett. 53 (2002) 385–391.
[18] R. Sanchez, J.A. Garcia, A. Medrano, M. Rico, R. Martinez, R. Rodriguez, C.F. Ramos, Successive ion implantation of high doses of carbon and nitrogen on steels, Surf. Coat. Technol. 158 (2002) 630–635.
[19] F.Z. Cui, Z.S. Luo, Biomaterials modification by ion-beam processing, Surf. Coat. Technol. 112 (1999) 278–285.
[20] J. Flis, J. Mankowski, T. Zakroczymski, The formation of phosphate coatings on nitrided stainless steel, Corros. Sci. 43 (2000) 1711–1725.
[21] N. Kumar, S. Kataria, S. Dash, S.K. Srivastava, C.R. Das, P. Chandramohan, et al., Tribological properties of nitrogen ion implanted steel, Wear 274 (2012) 60–67.
[22] A.V. Byeli, V.A. Kukareko, L.V. Boyarenko, A.A. Kolesnikova, Friction-induced microstructural variations in steels subjected to low-energy elevated-temperature nitrogen ion implantation, Wear 225 (1999) 1148–1158.
[23] R. Tapash, Rautray, R. Narayanan, K.-H. Kim, Ion implantation of titanium based biomaterials, Prog. Mater. Sci. 56 (2011) 1137–1177.
[24] H. Habazakia, Corrosion of amorphous and nanograined alloys Shreir's Corrosion, vol. 3, 2010, pp. 2192–2204.
[25] J.D. Bressan, D.P. Daros, A. Sokolowski, R.A. Mesquita, C.A. Barbosa, Influence of hardness on the wear resistance of 17-4 PH stainless steel evaluated by the pin-on-disc testing, J. Mater. Process. Technol. 205 (2008) 353–359.
[26] B.Q. Chen, Principle and Process of Modified Materials by Ion Beam, National Defense Industry Press, Beijing, 1995, pp. 157–160.
[27] G.B. Sigal, M. Mrksich, G.M. Whitesides, Effect of surface wettability on the adsorption of proteins and detergents, J. Am. Chem. Soc. 120 (1998) 3464–3473.
[28] S.H. Mollmanna, L. Jorgensena, J.T. Bukrinskyb, U. Elofsson, W. Norde, S. Frokjaer, Interfacial adsorption of insulin Conformational changes and reversibility of adsorption, Eur. J. Pharm. Sci. 27 (2006) 194–204.
[29] D. Sun, J.A. Wharton, R.J.K. Wood, The effects of protein and pH on the tribocorrosion performance of cast CoCrMo, Tribol. Mater. Surf. Interfaces 2 (2008) 150–160.
[30] Y. Yan, A. Neville, D. Dowson, Biotribocorrosion of CoCrMo orthopaedic implant materials Assessing the formation and effect of the biofilm, Tribol. Int. 40 (2007) 1492–1499.
[31] Y. Yan, A. Neville, D. Dowson, Tribo-corrosion properties of cobalt-based medical implant alloys in simulated biological environments, Wear 263 (2007) 1105–1111.